

Exploring the boundary of quantum correlations with coherent light

Zheng-Hao Liu,^{1,3,4,*} Yu Meng,^{1,3,*} Yu-Ze Wu,^{2,*} Ze-Yan Hao,^{1,3} Zhen-Peng Xu,^{5,†} Cheng-Jun Ai,⁴ Hai Wei,⁴ Kai Wen,^{4,‡} Jing-Ling Chen,^{6,§} Jie Ma,^{2,¶} Jin-Shi Xu,^{1,3,7,**} Chuan-Feng Li,^{1,3,7,††} and Guang-Can Guo^{1,3,7}

¹*CAS Key Laboratory of Quantum Information, University of Science and Technology of China, Hefei 230026, People's Republic of China*

²*School of Mathematical Sciences, University of Science and Technology of China, Hefei, China*

³*CAS Centre for Excellence in Quantum Information and Quantum Physics, University of Science and Technology of China, Hefei 230026, People's Republic of China*

⁴*Beijing QBoson Quantum Technology Co., Ltd., Beijing 100015, China*

⁵*Naturwissenschaftlich-Technische Fakultät, Universität Siegen, Walter-Flex-Straße 3, 57068 Siegen, Germany*

⁶*Theoretical Physics Division, Chern Institute of Mathematics, Nankai University, Tianjin 300071, People's Republic of China*

⁷*Hefei National Laboratory, University of Science and Technology of China, Hefei 230088, People's Republic of China*

(Dated: August 17, 2022)

Contextuality, a hallmark feature of the quantum theory, captures the incompatibility between quantum correlations and any noncontextual hidden-variable model. The Greenberger–Horne–Zeilinger (GHZ)-type paradoxes are proofs of contextuality which reveal this incompatibility with deterministic logical arguments. However, the simplest GHZ-type paradox with the fewest number of complete contexts and the largest degree of nonclassicality remains elusive. Here, we derive a GHZ-type paradox utilising only three complete contexts and show this number cannot be further reduced. We forward to demonstrating the paradox with an experiment which recovered all essential ingredients in a 37-dimensional contextuality test based on high-speed modulation, optical convolution and homodyne detection of time-multiplexed modes of coherent light that can be interpreted as a classical entity. By proposing and observing a strong form of contextuality in an extremely high-dimensional system, our results pave the way for the exploration of exotic quantum correlations with optical systems.

A long-standing question regarding the interpretation of the quantum theory is whether it gives a complete description of the nature [1]. In stark contrast to our customary intuition, not all properties have well-defined values in the quantum world. This apparent counter-intuition can be traced back to two origins. One is the incompatibility between observables: Heisenberg's uncertainty principle [2] famously dictates that noncommuting observables have no meaningful joint values; the other more subtle origin is the contextuality of quantum measurements, namely, it is not possible to specify the measurement outcome of an observable with any kind of hidden-variable, if the full set of compatible observables jointly measured are not specified [3]. Contextuality captures the most defining aspects of quantum correlations, which includes nonlocality as a special case in the multipartite scenario [4]; it has a wide spectrum of applications in quantum information tasks like randomness expansion [5–7], quantum state discrimination [8], dimension witnessing [9, 10] and self-testing [11]; more importantly, it has an intimate affiliation with the acceleration and universality of quantum computation [12–16].

Contextual correlations can manifest in different forms. While the violation of noncontextual inequalities is a common way of detecting contextuality, the logical proofs dubbed Greenberger–Horne–Zeilinger (GHZ)-type paradoxes [17, 18] can serve as a conceptually clear and mathematically strong [19] alternative. In a GHZ-type paradox, measurements of a specific quantum state on sets of rays cannot be assigned consistent noncontextual values, revealing contextuality without resorting to any inequality. The merit of a GHZ-type paradox is reflected by its simplicity, which can in turn be defined either by the number of rays used in the logical proof [20, 21] or the number of contexts [22], i.e., the orthonormal basis, that must be used to include all the rays. The significance of the latter definition is twofold: firstly, when transformed into noncontextual inequalities, a logical proof using fewer contexts yields a larger ratio of violation. Secondly, the quantum violation of the corresponding inequalities can be captured by a physical principle called exclusivity principle [23, 24], and the times to invoke the exclusivity principle in the demonstration of logical contextuality precisely equals the number of contexts in the proof. Therefore, the simplest logical proof of contextuality with a minimal number of context covers is not only a strong form of correlation but also an indication of nature's correlating power; this is especially the case in the light of that the interpretation of quantum correlations with physical principles is limited to very few cases [25]. However, after more than 30 years of GHZ's seminal work [17], the exact lower bound of context num-

* These authors contributed equally to this work.

† Zhen-Peng.Xu@uni-siegen.de

‡ wenk@boseq.com

§ chenjl@nankai.edu.cn

¶ jiema@ustc.edu.cn

** jsxu@ustc.edu.cn

†† cffi@ustc.edu.cn

ber in a GHZ-type paradox is still undetermined.

Here, we take a step towards answering the above question and observing the simplest and strongest form of logical contextuality. Specifically, our objective is to demonstrate a GHZ-type paradox formulated by only three groups of compatible observables, i.e., three contexts. We explicitly construct such a paradox by virtue of the graph-theoretic approach to quantum correlations [26], and prove its minimality in the sense that the number of contexts cannot be further reduced.

The constructed GHZ-type paradox requires a 37-dimensional Hilbert space. While such a system size is in principle amenable in multi-qubit platforms, the complicated form of the measurements and the stringent requirements of contextuality tests render direct experimental tests of the paradox extremely intractable. Despite all of these challenges, we were able to attest our theoretical findings with an optical demonstration. Our experiment was based on a proposal in Reference [27], which shows the equivalence between a standard contextuality test with sequential measurement and a simple prepare-and-measure experiment with some additional assumptions. We have emulated the prepare-and-measure of a qudit using high-speed electro-optical modulation, multiplication and convolution on temporal modes of coherent light in a fibre-based architecture. Moreover, we used homodyne detection to significantly expand the applicable Hilbert space dimension and achieve the desired high-dimensionality.

Our results elucidated the potential of the temporal-multiplexed optical system, which is already a leading architecture for coherent Ising machine [28–30] and continuous-variable measurement-based quantum computation [31–33], in investigating exotic quantum correlations. Such an investigation is possible because the physical principle of global exclusivity [23, 24] applies equally well in the classical domain [34], and the quantum coherence presenting in optical systems crucially guarantees the rules of probability calculation to be same as dictated by the Born’s rule. Because any Kochen–Specker set utilising n contexts implies the existence of a GHZ-type paradox with $n - 1$ contexts [21], our finding also paves the way to the search for a “simplest” Kochen–Specker set that might be included in only four independent contexts.

Contextuality without inequality

The GHZ-type paradoxes are extreme manifestations of quantum contextuality. They refer to scenarios where the quantum theory and any noncontextual model predict deterministically contradicting under the same conditions of observed data. Formally, a GHZ-type paradox can be expressed using the conditional probabilities as

follows:

$$\begin{aligned} \sum_{k=1}^{m_1} \Pr(1|[1, k]) &= 1, \\ \sum_{k=1}^{m_2} \Pr(1|[2, k]) &= 1, \\ &\dots \\ \sum_{k=1}^{m_{n-1}} \Pr(1|[n-1, k]) &= 1, \\ \hline \sum_{k=1}^{m_n} \Pr(1|[n, k]) &= \begin{cases} 0, & \text{NCHV,} \\ 1, & \text{Q.} \end{cases} \end{aligned} \quad (1)$$

where $1|[j, k]$ denotes an event where the outcome of the k -th projective measurement in the j -th context is 1, m_j is the number of measurements in the j -th context, $[j, k]$ can be converted to a single index $\sum_{i=1}^{j-1} m_i + k$, and n is the total number of contexts used in the paradox. The superscripts Q and NCHV indicate the probabilities will be calculated via the quantum theory and a noncontextual hidden-variable model, respectively. In layman’s terms, a GHZ-type paradox indicates some events deemed impossible by noncontextual models are bound to happen according to the quantum theory. In the Methods section, we will provide an explicit illustration using the original GHZ paradox.

The study of GHZ-type paradox benefits from multiple theoretical tools like the sheaf-theoretic approach [19, 35] and the graph states [36–38]. Here, our analysis will be mainly based on the graph-theoretic approach to contextuality [26] which uses a graph of exclusivity to capture the impossibility of some events taking place simultaneously (i.e., exclusivity). Concretely, the vertices $V(G)$ of the exclusivity graph G represent the events of observing certain measurement outcomes, and its edges $E(G)$ connect pairs of exclusive events. Once a graph of exclusivity is given, the sum of event probabilities in noncontextual and quantum theories will be bounded by graph constants, namely, the independence number and Lovász number [27, 39]:

$$\sum_{i \in V} \Pr(1|i) - \sum_{(i,j) \in E} \Pr(1, 1|i, j) \stackrel{\text{NCHV}}{\leq} \alpha(G) \stackrel{\text{Q}}{\leq} \vartheta(G). \quad (2)$$

Here, $\Pr(1, 1|i, j)$ is the probability of simultaneously observing events i, j ; this term compensates for the deviation from exclusivity [40]. Graphs with a large ratio ϑ/α thus have the merit of producing significant inconsistency between noncontextual and quantum theories.

Different from the above-mentioned inequality-based approach, in the GHZ-type paradoxes, contextuality is revealed by logical arguments and without inequality [41]. Here we show how such an approach—sometimes considered “the simplest form” [42] in the setting of Bell nonlocality, i.e., the contextuality in the multipartite scenario—can be related to the notion of the graph of exclusivity. According to the known conditional probabilities in Eq. (1), in every round of experiment, at most one events among $1|[j, k], k \in \{1, \dots, m_j\}$ will take place.

Therefore, events in the same context are mutually exclusive and thus form a clique in the graph of exclusivity. Applying the above argument on every sum of probabilities in Eq. (1), we find the graph of exclusivity G corresponding to these events has n cliques, and the chromatic number of its graph complement is also $\chi(\bar{G}) = n$; the detailed proof is deferred to the Methods section. Furthermore, summing over all the conditional probabilities and comparing the result with Eq. (2) yields $\alpha(G) = n - 1$, $\vartheta(G) = n$ which is the maximum allowed by the exclusivity principle, in other words, the quantum correlation associated with a GHZ-type paradox is also fully contextual [43].

A three-context GHZ-type paradox

Because the graphs of exclusivity in GHZ-type paradoxes have a fixed $\vartheta - \alpha = 1$, a GHZ-type paradox using fewer contexts is associated with a larger quantum-classical ratio and stronger nonclassicality. However, the fewest number of contexts required in a GHZ-type paradox is not known: obviously, it must be greater than 2, but every known example of GHZ-type paradox uses at least 4 contexts. Both noncontextuality inequality [44] and logical proofs of contextuality [45] using 3 contexts are well exploited in experiments [46–48], but the corresponding graph of exclusivity—a pentagon (cf. Fig. 1(a)), has only a $\vartheta - \alpha = \sqrt{5} - 2 < 1$, and the logical proof does not constitute a GHZ-type paradox since the quantum violation is less than 1. Furthermore, a GHZ-type paradox can be constructed from a Kochen–Specker set by removing one context and extra rays, while all known Kochen–Specker sets employ at least 5 contexts [49]. The graph of exclusivity, as shown in Fig. 1(b), coincides with which in the original GHZ paradox. All these observations make the search for a three-context GHZ-type paradox an interesting and crucial task.

To search for a three-context GHZ-type paradox, our starting point is its relationship with the graph of exclusivity of the paradox’s composing events. Specifically, such a graph of exclusivity G should have some fixed graph-theoretic constants, including an independence number of $\alpha(G) = 2$ and a Lovász number of $\vartheta(G) = 3$; moreover, its graph complement should have a chromatic number of $\chi(\bar{G}) = 3$, that is, \bar{G} is triangle-free and three-colourable. We have identified the graph complement of the Perkel graph [50] as shown in Fig. 1(c) as a competent candidate for the graph of exclusivity. Moreover, we prove in the Methods section that no strongly regular graph can satisfy all the above requirements, thus posing further limitations to the existence of other examples.

Once the candidate graph of exclusivity is determined, we can calculate the explicit form of the measurement events represented by a set of rays; each ray corresponds to the nondegenerate eigenstate of a projector. These rays form an orthogonal representation [51] of the Perkel graph. To obtain the orthogonal representation, the procedure is first to determine the Gram matrix of the

rays by semidefinite programming known as Lovász optimisation [39], and then to solve the individual rays by Cholesky decomposition and Gaussian elimination. We realised the semidefinite programming using a Python package `cvxopt` and the Cholesky decomposition using `Mathematica` 11.2. As the result, the form of the three-context GHZ-type paradox can be expressed as:

$$\begin{aligned} p_1 &:= \sum_{k=1}^{19} \Pr(1|k) = 1, \\ p_2 &:= \sum_{k=20}^{38} \Pr(1|k) = 1, \\ \hline p_3 &:= \sum_{k=39}^{57} \Pr(1|k) = \begin{cases} 0, & \text{NCHV,} \\ 1, & \text{Q.} \end{cases} \end{aligned} \quad (3)$$

The explicit definition of the individual rays, as well as the Gram matrix, will be given in the Extended Data Figure 1. Benefitted from the symmetry of the Perkel graph, the Gram matrix has a simple analytic form, and we were able to confirm that the rank of the matrix is 37, which is also the minimal state space dimension in which the constructed rays can be embedded.

A time-multiplexed optical test of contextuality

Our proposed three-context GHZ-type paradox is strong, both in the sense that it can be embedded in the least possible number of orthonormal basis and that a noncontextuality inequality with a high quantum-classical ratio of $3/2$ can be acquired from its comprised measurements. Moreover, according to the form of Eq. (3), to observe such a paradox experimentally, it is sufficient to measure the projection probability of

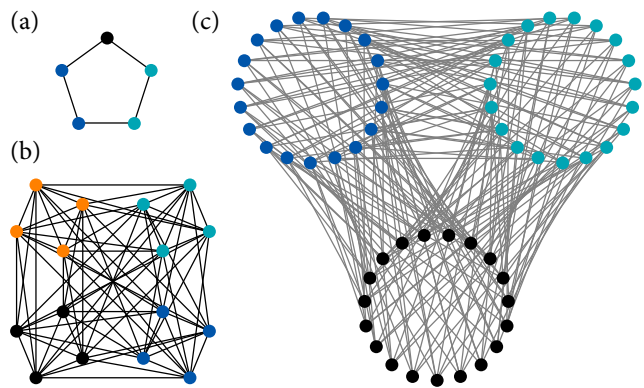


Fig. 1. **Graphs of exclusivity.** The vertices with the same colour are mutually connected and belong to the same context. (a) A pentagon is the simplest graph which shows nonclassicality when considered as a graph of exclusivity. Measurements with such an exclusivity structure exhibit a three-context Hardy-type paradox, but the quantum success probability is less than 1. (b) The graph complement of the Shrikhande graph is the underlying exclusivity structure of the original GHZ paradox with four contexts. (c) The orthogonal representation of the Perkel graph constitutes a GHZ-type paradox with three contexts. Note that the graph of exclusivity here is complementary to the Perkel graph and the grey lines connect the disjoint vertices.

the initial state on various measurement basis, and additionally to confirm the ideality of measurements, especially the orthogonality of measurements corresponding to mutually exclusive events. The procedure is akin to Cabello’s simplified method for testing contextuality using prepare-and-measure experiments [27] with graph-theoretic approach-based inequalities: as shown in Fig. 2(a) and (b), both have the merit of requiring no sequential, nondestructive measurements.

The most significant challenge for experimentally observing the three-context GHZ-type paradox thus boils down to the realisation of high-dimensional measurements. Due to the complicated form of the projectors, such measurements would require many entangling operations in a multi-qubit system and suffer from decreased accuracy. In contrast, high-dimensional systems are natively available in the optical domain, most prominently in the form of structured light [52–54]. Here, we shall explore an alternative approach—by using the time-bin degree of freedom of light—to implement an analogous prepare-and-measure experiment. The primary reason for choosing such a system as the experimental platform is the availability of a common phase reference, often called a “local oscillator” in the context of continuous-variable quantum optics. As we will elucidate below, it enables the extraction of coherent light’s amplitude and the decomposition of high-dimensional measurement into relatively low-dimensional subspaces, thus greatly facilitating the experiment.

Our time-multiplexed experiment relied on the following encoding to map a d -dimensional quantum state onto a series of pulsed coherent states:

$$|\mathbf{a}\rangle = (a_1 a_2 \cdots a_d)^\dagger \leftrightarrow \{|\alpha_1, \Delta t\rangle, |\alpha_2, 2\Delta t\rangle, \dots, |\alpha_d, d\Delta t\rangle\}, \quad (4)$$

where $\alpha_k = \tilde{\alpha} a_k$ denotes the displacement of the individual coherent states and $\tilde{\alpha}$ is a constant. The second entry of the coherent state specifies the time that it is generated. This coherent state train can be generated by casting intensity modulation on a pulsed laser. To measure the encoded state, we sent the pulse train into a fibre ring which has a round-trip time of Δt , so a pulsed coherent state met and interfered with another emitted at a later time after it circumnavigated the ring. The output modes from the ring thus acquired a component from the earlier pulses. Effectively, they experienced a discrete convolution and resembled a wavefunction $\mathbf{a} * \mathbf{c}$, with the kernel of convolution being $\mathbf{c} = \{c_1, c_2, \dots, c_d\}$ and c_k denoting the amplitude ejection ratio of a pulse upon its k -th encounter of the output coupler. The output pulse at time $d\Delta t$ thus had an amplitude of $\sum_{k=1}^d a_{d+1-k} c_k$, which is exactly the inner product $\langle \mathbf{c} | \mathbf{a} \rangle$, where $\mathbf{c} = \{c_d, c_{d-1}, \dots, c_1\}$ represents the entry-reversed kernel of convolution, and can be further adjusted by intensity modulation outside the fibre ring. Therefore, the probability of a qudit measurement can be efficiently evaluated by monitoring the strength of the output pulse at a specific timestamp.

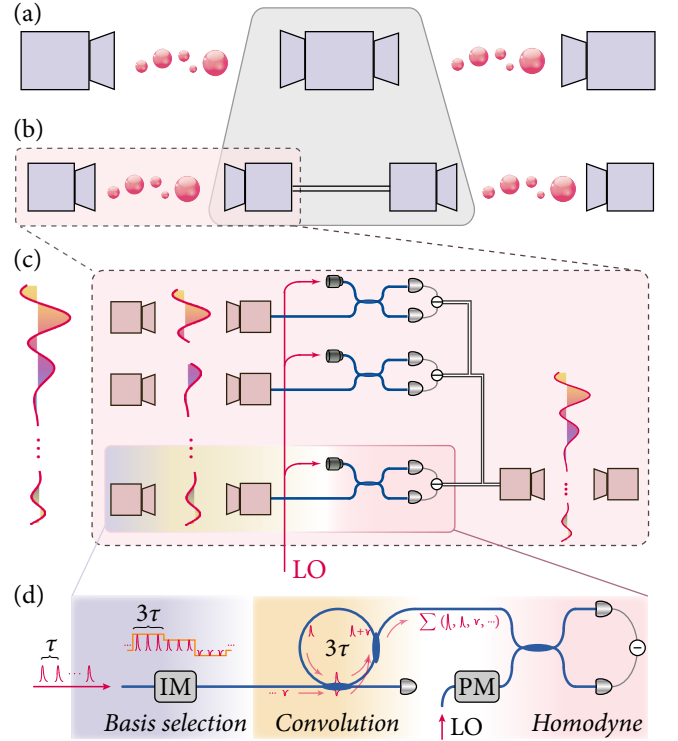


Fig. 2. Experimental design. (a) A standard test of contextuality features at least one sequential nondestructive measurement. (b) By assuming the Lüder’s rule, a nondestructive measurement can be replaced by a destructive measurement and a subsequent re-preparation according to the measurement result. (c) When the quantum state is replaced by modes of coherent light, the prepare-and-measure can be disassembled into different subspaces and realised separately, with the assistance of a common phase reference. (d) Sketch of the experimental setup. An intensity modulator prepared various input states. A fibre ring implemented optical convolution. The output mode at a specific time corresponded to the post-measurement state, whose amplitude was subsequently extracted via homodyne detection. IM intensity modulator, PM phase modulator, LO local oscillator.

In practice, the fibre ring is inevitably accompanied by ejection into unwanted timestamps, insertion losses and chromatic dispersion, so the ejection ratio quickly decreases for more loops. As such, the kernel of convolution cannot have a lot of meaningfully nonzero terms, hampering the capability of measuring high-dimensional states. However, this can be greatly remedied by replacing photodetection with balanced homodyne detection. By interfering the optical mode to be measured with the local oscillator on a balanced beam splitter, the intensity difference between the two output ports recorded as a photocurrent will be proportional to the mode’s amplitude in-phase with the local oscillator. Since the projectors in the three-context GHZ-type paradox (Eq. (3)) do not comprise a single complex number, the in-phase amplitude can already capture all information of the coherent states after convolution.

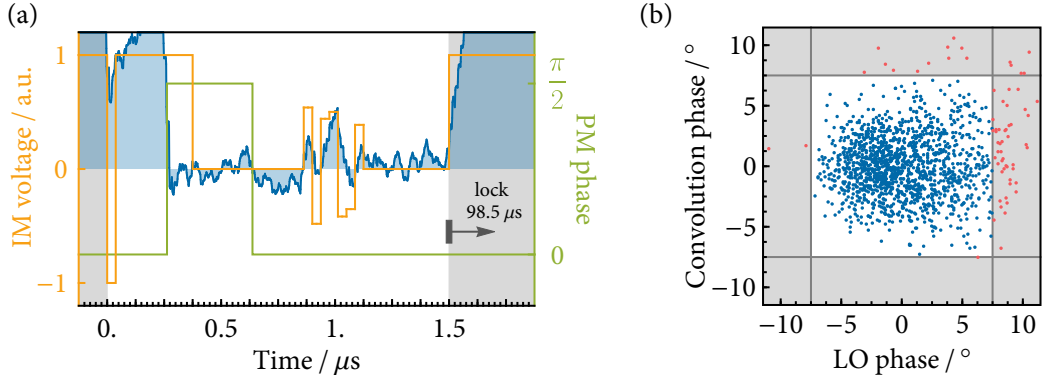


Fig. 3. **Data acquisition.** (a) An exemplary control signal and recorded waveform. The control signal consists of an intensity notch for synchronisation, a $\pi/2$ -pulse at the local oscillator for phase calibration, and the intensity modulations encoding the preparation and convolution basis. (b) Measured phase error of the convolution fibre ring and the local oscillator. The red-coloured data points had at least one phase error greater than $\pi/24$ and were excluded from the final calculation.

With the amplitude information available, we are in the position to divide-and-conquer the measurement of a high-dimensional state. The procedure is shown in Fig. 2(c). Firstly, we expressed the state $|\psi\rangle$ as the direct sum of some decomposed, unnormalised states living in lower-dimensional subspaces: $\psi = \bigoplus_{k=1}^b \mathbf{a}_k$, where b is the total number of partitions. For each lower-dimensional state \mathbf{a}_k , we employed the optical convolution with the kernel being \mathfrak{a}_k and homodyne detection as described above to register the amplitude on the desired measurement basis. Secondly, a b -dimensional state also represented by pulsed coherent light was re-prepared; its entries were specified by the corresponding amplitudes registered in the previous round. Again using optical convolution, we measured the sum of the b -amplitudes as the photocurrent at homodyne detection. The total of the amplitude is thus proportional to the inner product $\langle \phi | \psi \rangle$, where the projector is related to the kernels of convolution by $\phi = \bigoplus_{k=1}^b \mathfrak{a}_k$. Finally, the measurement probability was calculated as the absolute square of the photocurrent normalised against a set of orthonormal basis.

Experimental implementation

We realised the prepare-and-measure procedure with a high-speed electro-optical modulation platform as shown in Fig. 2(d); the detailed experimental setup will be deferred to the Extended Data Figure 2. We have exploited a MATLAB 2020b script to control an arbitrary function generator and a digital oscilloscope to run a fully automated experiment. A frequency-locked fibre laser with a repetition rate of $1/\tau = 75.91$ MHz, a central wavelength of 1560 nm and a spectral bandwidth of 12 nm was adopted as the source of pulsed coherent states. From the parameters of the laser, we estimate the maximal displacement of the coherent state as $\tilde{\alpha} = 1.014 \times 10^4$, so the shot noise from the fluctuation of photon numbers between individual pulses are comparatively small.

The 37-dimensional state was encoded in six direct sum

subspaces in our experiment; each of the subspaces was in turn represented by seven pulsed coherent states. To implement both the preparation of the initial state and the adjustment of the convolution basis, we utilised a commercial lithium niobate intensity modulator with a power extinction ratio of 28 dB. The intensity modulator only generated preparation and measurement bases with real coefficients, but it can be easily upgraded to realise complex coefficients by employing an additional phase modulator. Due to the non-vanishing width of the rising and falling edges of the arbitrary function generator measured as 7 ns, we always modulated three consecutive pulses and only measured the amplitude of the middle one to avoid clashing with the modulation edges; this resulted in a modulation period of $\Delta t = 3\tau$.

To construct the fibre ring for convolution, we utilised two fibre beamsplitters with an amplitude splitting ratio of 90:10 and a free-space delay line. The length of the delay line was carefully adjusted in order to align the ring length to 3τ and maximise the interference visibility. We have manually calibrated the kernel of convolution instead of using the round-trip loss of the fibre ring cavity (which is estimated to be 27%) as the pulses emitted from the ring after different numbers of circulation had different chromatic dispersion and thus non-identical interference visibility with the local oscillator. The balanced homodyne detector used in our experiment had a linear response to power difference up to $5 \mu\text{W}$ as shown in Extended Data Figure 3, and all experimental points fell well in the linear range.

Active phase stabilisation was a crucial part of our experiment for correct data acquisition. We used a photodetector at the second output port of the convolution ring's injection fibre coupler and an additional output of the balanced homodyne detector to monitor the phase of the convolution ring and the local oscillator, respectively. A Laselock model was adopted as the phase locking servo and drove the piezo-mounted mirrors in the free-space session and a fibre stretcher for feedback con-

trol. The phase locking and data acquisition was based on a sample–hold scheme depicted in Fig. 3(a). In the first $98.5 \mu\text{s}$ of a cycle, the intensity modulator was set at maximal transmissivity, and the servo implements active phase stabilisation by the Pound–Drever–Hall locking technique. In the last $1.5 \mu\text{s}$, the electro-optic modulators delivered various modulations; the phases were kept constant as the piezos in the feedback circuits would not respond to such a high-frequency disturbance. For each data measured, we verified the locking phase by adding a $\pi/2$ phase on the local oscillator before the prepare-and-measure pulses and observing the response from the homodyne detector. The result of phase calibration is shown in Fig. 3(b). The standard deviations of the convolution phase and the local oscillator phase error were measured to be 2.74° and 3.94° . Additionally, we have discarded all data points with at least one phase error greater than 7.5° to avoid undesired noise.

By virtue of the precise electro-optical modulation and phase-locking, the obtained measurement probabilities closely resembled that would be in an ideal quantum prepare-and-measure experiment. The ideality can be best witnessed in that when the state rays corresponded to prepare and measure procedures were orthogonal, the resulted homodyne detection amplitude would almost completely vanish. We have confirmed the above witness by implementing the prepare-and-measure procedure corresponding to every pair of exclusive rays and projectors in the orthogonal representation of the Perkel graph. Note that the procedures were not implemented if at least one of the prepared or measured rays equalled the computational basis; in which case the probability would only depend on the extinction ratio of intensity modulation and not on interference. The results for the remaining events (cf. Fig. 4(a)) demonstrated an average detection probability for such a procedure was only $1.74(11)\%$. Henceforth, the error bars corresponding to 1σ standard deviations were obtained from bootstrapping. The high orthogonality ensured the statistics from our prepare-and-measure procedure conform to the requirements of exclusivity specified by the Perkel graph, so the prerequisites of the theoretical arguments were actually fulfilled on this platform.

Next, we proceed to test the three-context GHZ-type paradox by directly measuring the three sums of probabilities in Eq. (3). Our experimental result gives:

$$p_1 = 0.9939(15), \quad p_2 = 0.9980(2), \quad p_3 = 0.9983(2). \quad (5)$$

It was in excellent accord with quantum predictions and displayed strong disagreement with the prediction of the noncontextual theories.

Further, we complemented the observation GHZ-type paradox with a test of the noncontextual inequality associated with the same graph of exclusivity. Violation of such an inequality compensates for the deviation from ideal exclusivity and can refute noncontextual models with realistic experimental data [27]. From the verification of orthogonality we deduced the second term in

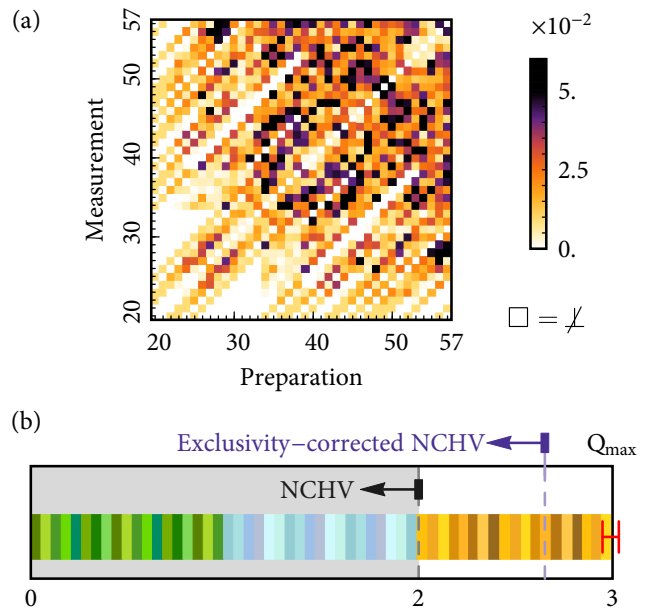


Fig. 4. **Experimental results.** (a) Calculated values of the second term in (2) for each pair of compatible projectors that does not equal the computational basis. The colours stand for the probabilities of ideally orthogonal measurements not giving exclusive responses. (b) Experimental results for the three-context GHZ-type paradox contrasted with the predictions of noncontextual models, exclusivity-corrected noncontextual models and the quantum theory. The three coloured bands correspond to the three sums of probabilities in Eq. (3), respectively.

Eq. (2) to be $0.651(40)$. As shown in Fig. 4(b)), by adding this term of compensation to the independence number, we found that after correcting for the non-ideal exclusivity, the experimental data still violated the upper bound of noncontextuality by 8.06 standard deviations and thus rejecting such a description with almost absolute confidence.

In conclusion, we have demonstrated the potential of optical interferometry for the exploration of some most exotic quantum correlations. First, by extending the graph-theoretical approach to the study of the GHZ-type paradoxes, we have found a strong logical argument of contextuality that uses only three contexts—least possible number of contexts in theory—to reveal a deterministical contradiction between classical and quantum descriptions of the same underlying correlations. When translated into experimentally testable noncontextual inequality, the argument also gives the largest quantum–classical ratio among all GHZ-type paradoxes. Interestingly, the argument was found by examining named graphs with known graph-theoretic constants, instead of using the modern computer-assisted search method [21, 40] or being derived from a Bell inequality already with a large quantum violation. In fact, with a chromatic number less than 4, the graph of exclusivity here cannot host any Bell-type experiment. Therefore,

our result highlights the interdisciplinary link between the most exotic quantum correlations and graphs with high degrees of symmetry, and may shed new light on the search for other strong forms of quantum correlations.

Secondly, we have exploited a time-multiplexed optical setup to experimentally tested the three-context GHZ-type paradox. Implementing a 37-dimensional prepare-and-measure experiment with precision high enough to demonstrate contextuality is extremely challenging; nonetheless, we circumvented the obstacles by resorting to a less technically demanding method to recover all the key ingredients for demonstrating the three-context GHZ-type paradox, including the exclusivity between mutually orthogonal measurements and the quantum statistics in stark contrast with its noncontextual counterparts. The essence of our method was the correspondence between a qudit state and a train of pulsed coherent light and, more significantly, the direct sum decomposition of a high-dimensional state into lower-dimensional components. Time-multiplexing is a widely adopted method in large-scale entanglement generation for quantum computation [55, 56] where the state space is composed in a direct product fashion. Here, we have provided another approach to composing the state space and elucidated its compatibility with homodyne measurement. We anticipate the approach could stimulate the development of novel protocols and realisations of high-dimensional quantum information processing.

Our experiment only adopted strong coherent light from a pulsed laser instead of any nonclassical light source, yet it was still able to demonstrate the quantum phenomenon of contextuality. The reasons are twofold, that the Kochen–Specker contextuality is measurement-related and does not rely on specific quantum resources like entanglement to manifest, and that the detection probability of light on a specific mode is determined by the same mathematical rule as the Born rule: as the latter already implies contextuality [57], the former as a quantum simulator must behave the same [58]. On the other hand, also because lacking the use of entanglement, all the effects observed in our experiment are classically simulable and requires only a moderate memory cost [59] as the primary resource overhead. However, the optical setup here is versatile, reconfigurable, and compatible with nonclassical photon sources like the optical parametric oscillator and non-Gaussian operations like photon-number resolution [60]. It is thus plausible the photonic setup will be capable of exploring other more complicated quantum correlations once it is supplemented with appropriate resources.

We believe this work has opened several new avenues for future research. From a fundamental perspective, the existence of a three-context GHZ-type paradox leaves open the possibility of finding a Kochen–Specker set that can be covered by four contexts. It would be interesting to consider if such a set can already be constructed as a state-independent version of the GHZ-type paradox here, using some methods of expansion, e.g., as in

Reference [61]. Pertinent to this topic, we also prove in the Methods section that if any four-context Kochen–Specker set does exist then the four contexts must be disjoint; consequently, this Kochen–Specker set would not accept a simple parity proof [20, 22]. On the applied side, the time-multiplexed optical platform has found applications in synthetic dimension-based quantum simulation [62, 63]. It would be beneficial also to adopt homodyne measurement in these works to detect the phase information and reveal more complicated quantum dynamic features. Moreover, the direct sum and product encoding could be combined to study the dynamics of high-dimensional, many-body systems. Finally, our experiment relies on an additional assumption, that is, the equivalence between the Born’s rule and the rule of optical wave interference. A future experiment using quantum entities to implement a genuine contextuality test would thus be highly desirable for investigating the law of nature and taking the full power of contextuality in quantum information tasks.

Methods

The GHZ paradox and its probability form. Consider the following Pauli product measurements on a three-qubit system: $\mathcal{M}_1 = \sigma_x^{(1)} \sigma_y^{(2)} \sigma_y^{(3)}$, $\mathcal{M}_2 = \sigma_y^{(1)} \sigma_x^{(2)} \sigma_y^{(3)}$, $\mathcal{M}_3 = \sigma_y^{(1)} \sigma_y^{(2)} \sigma_x^{(3)}$, and $\mathcal{M}_4 = \sigma_x^{(1)} \sigma_x^{(2)} \sigma_x^{(3)}$. If the system is initiated at a state so the measurement outcome of $\mathcal{M}_1, \mathcal{M}_2$ and \mathcal{M}_3 are all +1, then a noncontextual theory will predict the measurement of \mathcal{M}_4 on the system definitely returns +1, because the assumption of noncontextuality means the outcome of measuring $\sigma_x^{(1)}$ will not depend on whether it is measured with $\sigma_x^{(2)} \sigma_x^{(3)}$ as in \mathcal{M}_0 or $\sigma_y^{(2)} \sigma_y^{(3)}$ as in \mathcal{M}_1 ; this is similar for $\sigma_x^{(2)}, \sigma_x^{(3)}$. Taking into account the involutory of Pauli operators, the outcome of \mathcal{M}_0 in such theories will be the product of $\mathcal{M}_1, \mathcal{M}_2$ and \mathcal{M}_3 that is +1. However, quantum theory is contextual: the only three-qubit state $|\psi\rangle$ giving $\langle \mathcal{M}_1 \rangle_\psi = \langle \mathcal{M}_2 \rangle_\psi = \langle \mathcal{M}_3 \rangle_\psi = +1$ is the GHZ state $|\psi\rangle = |\text{GHZ}\rangle = (|000\rangle - |111\rangle)/\sqrt{2}$, which satisfies $\langle \mathcal{M}_4 \rangle_{\text{GHZ}} = -1$.

Each of the four Pauli product measurements is composed of three local dichotomic measurements. If the outcomes of \mathcal{M}_1 through \mathcal{M}_4 are specified as in the above GHZ paradox, then the local dichotomic measurements corresponding to each Pauli product measurement will have four possible combinations. For example, $\mathcal{M}_4 = -1$ implies either $\sigma_x^{(1)} = \sigma_x^{(2)} = \sigma_x^{(3)} = -1$, or that one and only one local measurement among $\sigma_x^{(1)}, \sigma_x^{(2)}$ and $\sigma_x^{(3)}$ evaluates to -1 . Let $\Pi_\mu^{\pm(\nu)} = (\mathbb{1} \pm \sigma_\mu^\nu)/2$, then the four elementary events can be expressed as:

$$\begin{aligned} 1|[4, 1] : &= 1 |\Pi_x^{-(1)} \otimes \Pi_x^{-(2)} \otimes \Pi_x^{-(3)}, \\ 1|[4, 2] : &= 1 |\Pi_x^{-(1)} \otimes \Pi_x^{+(2)} \otimes \Pi_x^{+(3)}, \\ 1|[4, 3] : &= 1 |\Pi_x^{+(1)} \otimes \Pi_x^{-(2)} \otimes \Pi_x^{+(3)}, \\ 1|[4, 4] : &= 1 |\Pi_x^{+(1)} \otimes \Pi_x^{+(2)} \otimes \Pi_x^{-(3)}. \end{aligned} \quad (6)$$

In the same vein, we can define the elementary events $1|[j, k], j \in \{1, 2, 3\}, k \in [1, 4]$. The graph of exclusivity for all these events, as discussed in the main text, is the graph complement of the Shrikhande graph, so the total number of events that are allowed to happen according to any noncontextual model is no more than 3 for any initial state. That is, given $\sum_{k=1}^4 \Pr(1|[j, k]) = 1, j \in \{1, 2, 3\}$ it must be $\sum_{k=1}^4 \Pr(1|[4, k]) \stackrel{\text{NCHV}}{=} 0$. However, according to the calculated quantum expectations, the total probabilities of all the four groups of events will saturate the upper bound allowed by the principle of exclusivity, that is, $\sum_{k=1}^4 \Pr(1|[j, k]) \stackrel{\text{Q}}{=} 1, j \in [1, 4]$. This completes the transformation of the original GHZ paradox into the probability form as in Eq. (1).

Graph-theoretic constants in the GHZ-type paradoxes. Here we show that, suppose all the measurement rays in a GHZ-type paradox can be contained in n -contexts, then the corresponding graph of exclusivity G has $\alpha(G) = n - 1, \vartheta(G) = n$ and $\chi(\bar{G}) = n$. The first two equations can be justified by adding all the conditional probabilities together and comparing the sum with Eq. (2). To prove the last equation, we observe that \bar{G} can be coloured by assigning the same colour to all vertices that belong to a clique in G and using a different colour for each clique. This explicit construction guarantees $\chi(\bar{G}) \leq n$. But according to Lovász's celebrated sandwich theorem [64], $\chi(\bar{G}) \geq \vartheta(G) = n$, so it must be $\chi(\bar{G}) = n$.

No strongly regular graph hosts three-context GHZ-type paradox. A strongly regular graph with four parameters n, k, a and c , denoted by $\text{SRG}(n, k, a, c)$, is a n -vertex k -regular graph such that every two adjacent vertices have a common neighbours, and that every two non-adjacent vertices has c common neighbours. The theory of strongly regular graphs was introduced by Bose [65] in 1963 and was then used in many different mathematical fields, such as partial geometry [65], group theory [66] and coding theory [67].

Before proving the main lemma, let us list out some necessary symbols. For any graph G , we use $A(G), \alpha(G), \omega(G), \chi(G)$ and $\vartheta(G)$ to denote its adjacent matrix, independence number, clique number, chromatic number and Lovász number, respectively.

Lemma 1. There is no strongly regular graph with clique number 2 and chromatic number 3 such that the Lovász number of its complement graph is 3.

Proof. Suppose that there exists a strongly regular graph $G = \text{SRG}(n, k, a, c)$ satisfying $\omega(G) = 2, \chi(G) = 3$ and $\vartheta(\bar{G}) = 3$. Note that as $\omega(G) = 2$, we have $a = 0$.

We will first establish an inequality that $c \leq k \leq 2c + 3$. Let $A = A(G)$. We will consider the entries of A^2 . For any two vertices i and j , $(A^2)_{ij}$ is the number of walks of length 2 which starts at i and ends at j . So for adjacent vertices i and j , $(A^2)_{ij} = 0$ because i and

j has no common neighbours. For non-adjacent vertices i and j , $(A^2)_{ij} = c$ because i and j has exactly c common neighbours. And for any vertex i , $(A^2)_{ii} = k$ because G is a k -regular graph. Therefore, we have $A^2 = c(J - A) + (k - c)I$, where J is the $n \times n$ matrix with all entries equal to 1 and I is the $n \times n$ identity matrix. This implies that A has exactly three different eigenvalues k, λ_1, λ_2 such that λ_1 and λ_2 are the roots of $\lambda^2 + c\lambda - (k - c) = 0$. Therefore $\lambda_1 = \frac{-c - \sqrt{c^2 + 4(k - c)}}{2}$, and $\lambda_2 = \frac{-c + \sqrt{c^2 + 4(k - c)}}{2}$. The famous Hoffman–Delsarte [68, 69] eigenvalue bound says that for n -vertex k -regular graph H , we have $\alpha(H) \leq \frac{-\tau}{k - \tau}n$, where τ is the smallest eigenvalue of $A(H)$. Using this bound, we have $\alpha(G) \leq \frac{-\lambda_1}{k - \lambda_1}n$. Since $\alpha(G)\chi(G) \geq n$, we get an inequality $3 = \chi(G) \geq \frac{k - \lambda_1}{-\lambda_1} = \frac{2k + c + \sqrt{c^2 + 4(k - c)}}{c + \sqrt{c^2 + 4(k - c)}}$. By solving this inequality, we have $c + 2 - \sqrt{c^2 + 4} \leq k \leq c + 2 + \sqrt{c^2 + 4}$. Since k, c are non-negative integers and $c \leq k$, we now have

$$c \leq k \leq 2c + 3. \quad (7)$$

Next we show that in fact k only can be two possible integer values, namely $k \in \{c, 2c + 1\}$, by considering the multiplicities of λ_1 and λ_2 . Let m_i be the multiplicity of λ_i for $i \in \{1, 2\}$. Since the multiplicity of k is one, we have $m_1 + m_2 = n - 1$; also by considering the trace of A , we get $m_1\lambda_1 + m_2\lambda_2 + k = 0$. Solving the above two equations, we obtain that

$$m_1 = \frac{(n - 1)\lambda_2 + k}{\lambda_2 - \lambda_1} = \frac{n - 1}{2} + \frac{-k^2 + (2 - c)k}{2\sqrt{c^2 + 4(k - c)}}. \quad (8)$$

As m_1 is an integer, we conclude that $\sqrt{c^2 + 4(k - c)}$ must be an integer. Using $c \leq k \leq 2c + 3$, we have $c \leq \sqrt{c^2 + 4(k - c)} \leq \sqrt{c^2 + 4c + 12} < c + 4$. So $\sqrt{c^2 + 4(k - c)} \in \{c, c + 1, c + 2, c + 3\}$. An easy analysis shows that $k \in \{c, 2c + 1\}$.

By considering the number of paths of length 2 with a fixed an endpoint in G , we have an equality $(n - k - 1)c = k(k - 1)$. Therefore, $n = 2c$ when $k = c$, and $n = 6c + 4$ when $k = 2c + 1$. That is, G is either $\text{SRG}(2c, c, 0, c)$ or $\text{SRG}(6c + 4, 2c + 1, 0, c)$. In the former case, $G = \text{SRG}(2c, c, 0, c)$ must be a complete bipartite graph such that each part has exactly c vertices. Therefore $\chi(G) = 2$, a contradiction. So from now on, we only need to consider the later case $G = \text{SRG}(6c + 4, 2c + 1, 0, c)$.

We first consider the cases when $c \leq 2$. If $c = 0$, then G is exactly a single edge, implying that $\chi(G) = 2$, a contradiction. If $c = 1$, then $G = \text{SRG}(10, 3, 0, 1)$ is unique, i.e., the famous Peterson graph [70]. So we have $\vartheta(\bar{G}) = \frac{5}{2}$ [39] which is again a contradiction. If $c = 2$, then $G = \text{SRG}(16, 5, 0, 2)$ is also unique, i.e., the famous Clebsch graph [71]. In this case, we have $\chi(G) = 4$, a contradiction.

It remains to show that $G = \text{SRG}(6c + 4, 2c + 1, 0, c)$ does not exist for $c \geq 3$. Suppose such G exists. Take an arbitrary vertex v in G . Let $N(v)$ denote the set of

neighbours of v , and V_1 denote the non-neighbours of v . As G has no triangles, $N(v)$ is an independent set of size $2c + 1$ and $|V_1| = 4c + 2$. By the properties of strongly regularity of G , any vertex w in $N(v)$ has exactly $2c$ neighbours in V_1 , and any vertex u in V_1 has exactly c neighbours in $N(v)$ and $c + 1$ neighbours in V_1 .

Fix a vertex u in V_1 . Because $c \geq 3$, we can take three different neighbours w_1, w_2, w_3 of u in $N(v)$. Let W_i denote the set of the neighbours of w_i except v for all $i \in \{1, 2, 3\}$. Then $W_i \subseteq V_1$ and W_i is an independent set of size $2c$ for all $i \in \{1, 2, 3\}$. Moreover, if z is a neighbour of u in V_1 , z cannot be a neighbour of either w_1, w_2 or w_3 . So we have $N(u) \cap V_1 \subseteq V_1 \setminus (W_1 \cup W_2 \cup W_3)$. Since any two non-adjacent vertices in G have exactly c common neighbours and v is a common neighbour of w_1, w_2 and w_3 , we have $|W_1 \cap W_2| = c - 1$ and $|W_3 \cap (W_1 \cup W_2)| \leq |W_3 \cap W_1| + |W_3 \cap W_2| = 2c - 2$. Therefore $|W_1 \cup W_2| = 3c + 1$ and thus $|W_1 \cup W_2 \cup W_3| \geq (3c + 1) + 2c - (2c - 2) = 3c + 3$. Finally, we can reach a contradiction by the following inequality:

$$\begin{aligned} c + 1 &= |N(u) \cap V_1| \leq |V_1 \setminus (W_1 \cup W_2 \cup W_3)| \\ &\leq (4c + 2) - (3c + 3) = c - 1. \end{aligned} \quad (9)$$

The proof is now complete. \square

Disjointedness of four-context Kochen–Specker set. It has been proven in Reference [21] that there should be at least 4 complete contexts in Kochen–Specker set if all the contexts are disjoint. Here, we shall prove the inverse proposition explicitly stated in the following lemma.

Lemma 2. If there is a Kochen–Specker set consisting of only 4 complete contexts, then those contexts are all disjoint.

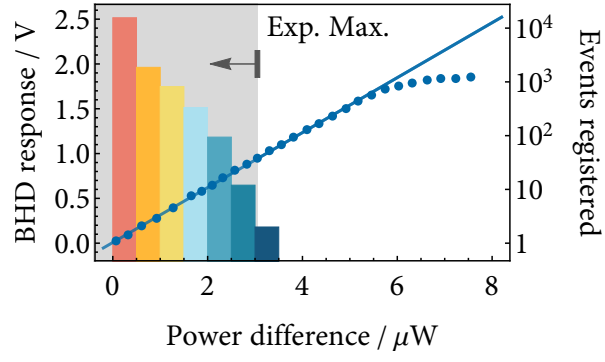
Proof. We prove it by contradiction. Let the four complete contexts be $\{C_i\}_{i=1}^4$. Without loss of generality, we can assume $C_1 \cap C_2 \neq \emptyset$ and $v_0 \in C_1 \cap C_2$. According to the relation between GHZ-type proof and Kochen–Specker set [21], we can obtain the exclusivity graph G of a GHZ-type proof by removing v_0 and other vertices connected to v_0 , especially all other vertices in C_1 and C_2 . Consequently, this exclusivity graph G can be covered by two cliques, which implies that $\vartheta(G) \leq 2$. Since it stands for a GHZ-type proof, $\alpha(G)$ should be strictly less than $\vartheta(G)$, thus the only possibility is that $\alpha(G) = 1$. However, this can only happen in the case that the graph can be covered by one clique, where $\vartheta(G) = \alpha(G) = 1$. This contradicts with the conclusion that G is the exclusivity graph of a GHZ-type proof. \square

-
- [1] A. Einstein, B. Podolsky, and N. Rosen, *Can quantum-mechanical description of physical reality be considered complete?*, *Phys. Rev.* **47**, 777 (1935).
 - [2] W. Heisenberg, *Über den anschaulichen inhalt der quantentheoretischen kinematik und mechanik*, *Z. Physik* **43**, 172 (1927).
 - [3] S. Kochen and E. P. Specker, *The problem of hidden variables in quantum mechanics*, *J. Math. Mech.* **17**, 59 (1967).
 - [4] A. Cabello, *Bell non-locality and Kochen–Specker contextuality: How are they connected?*, *Found. Phys.* **51**, 61 (2021).
 - [5] A. A. Abbott, C. S. Calude, J. Conder, and K. Svozil, *Strong Kochen–Specker theorem and incomputability of quantum randomness*, *Phys. Rev. A* **86**, 062109 (2012).
 - [6] M. Um, Q. Zhao, J. Zhang, P. Wang, Y. Wang, M. Qiao, H. Zhou, X. Ma, and K. Kim, *Randomness expansion secured by quantum contextuality*, *Phys. Rev. Applied* **13**, 034077 (2020).
 - [7] M.-H. Li, X. Zhang, W.-Z. Liu, S.-R. Zhao, B. Bai, Y. Liu, Q. Zhao, Y. Peng, J. Zhang, Y. Zhang, *et al.*, *Experimental realization of device-independent quantum randomness expansion*, *Phys. Rev. Lett.* **126**, 050503 (2021).
 - [8] D. Schmid and R. W. Spekkens, *Contextual advantage for state discrimination*, *Phys. Rev. X* **8**, 011015 (2018).
 - [9] O. Gühne, C. Budroni, A. Cabello, M. Kleinmann, and J.-Å. Larsson, *Bounding the quantum dimension with contextuality*, *Phys. Rev. A* **89**, 062107 (2014).
 - [10] M. Ray, N. G. Boddu, K. Bharti, L.-C. Kwek, and A. Cabello, *Graph-theoretic approach to dimension witnessing*, *New J. Phys.* **23**, 033006 (2021).
 - [11] K. Bharti, M. Ray, A. Varvitsiotis, N. A. Warsi, A. Cabello, and L.-C. Kwek, *Robust self-testing of quantum systems via noncontextuality inequalities*, *Phys. Rev. Lett.* **122**, 250403 (2019).
 - [12] J. Anders and D. E. Browne, *Computational power of correlations*, *Phys. Rev. Lett.* **102**, 050502 (2009).
 - [13] R. Raussendorf, *Contextuality in measurement-based quantum computation*, *Phys. Rev. A* **88**, 022322 (2013).
 - [14] M. Howard, J. Wallman, V. Veitch, and J. Emerson, *Contextuality supplies the ‘magic’ for quantum computation*, *Nature* **510**, 351 (2014).
 - [15] S. Bravyi, D. Gosset, and R. König, *Quantum advantage with shallow circuits*, *Science* **362**, 308 (2018).
 - [16] S. Bravyi, D. Gosset, R. Koenig, and M. Tomamichel, *Quantum advantage with noisy shallow circuits*, *Nat. Phys.* **16**, 1040 (2020).
 - [17] D. M. Greenberger, M. A. Horne, and A. Zeilinger, in *Bell’s theorem, quantum theory and conceptions of the universe* (Springer, 1989) pp. 69–72.
 - [18] N. D. Mermin, *Simple unified form for the major no-hidden-variables theorems*, *Phys. Rev. Lett.* **65**, 3373 (1990).
 - [19] S. Abramsky and A. Brandenburger, *The sheaf-theoretic structure of non-locality and contextuality*, *New J. Phys.* **13**, 113036 (2011).
 - [20] A. Cabello, J. Estebaranz, and G. García-Alcaine, *Bell–Kochen–Specker theorem: A proof with 18 vectors*, *Phys. Lett. A* **212**, 183 (1996).
 - [21] Z.-P. Xu, J.-L. Chen, and O. Gühne, *Proof of the Peres conjecture for contextuality*, *Phys. Rev. Lett.* **124**, 230401

- (2020).
- [22] P. Lisoněk, P. Badziag, J. R. Portillo, and A. Cabello, *Kochen–Specker set with seven contexts*, *Phys. Rev. A* **89**, 042101 (2014).
 - [23] A. Cabello, *Simple explanation of the quantum violation of a fundamental inequality*, *Phys. Rev. Lett.* **110**, 060402 (2013).
 - [24] B. Yan, *Quantum correlations are tightly bound by the exclusivity principle*, *Phys. Rev. Lett.* **110**, 260406 (2013).
 - [25] M. Pawłowski, T. Paterek, D. Kaszlikowski, V. Scarani, A. Winter, and M. Żukowski, *Information causality as a physical principle*, *Nature* **461**, 1101 (2009).
 - [26] A. Cabello, S. Severini, and A. Winter, *Graph-theoretic approach to quantum correlations*, *Phys. Rev. Lett.* **112**, 040401 (2014).
 - [27] A. Cabello, *Simple method for experimentally testing any form of quantum contextuality*, *Phys. Rev. A* **93**, 032102 (2016).
 - [28] P. L. McMahon, A. Marandi, Y. Haribara, R. Hamerly, C. Langrock, S. Tamate, T. Inagaki, H. Takesue, S. Utsunomiya, K. Aihara, *et al.*, *A fully programmable 100-spin coherent Ising machine with all-to-all connections*, *Science* **354**, 614 (2016).
 - [29] T. Inagaki, Y. Haribara, K. Igarashi, T. Sonobe, S. Tamate, T. Honjo, A. Marandi, P. L. McMahon, T. Umeki, K. Enbutsu, *et al.*, *A coherent Ising machine for 2000-node optimization problems*, *Science* **354**, 603 (2016).
 - [30] T. Honjo, T. Sonobe, K. Inaba, T. Inagaki, T. Ikuta, Y. Yamada, T. Kazama, K. Enbutsu, T. Umeki, R. Kasa-hara, *et al.*, *100,000-spin coherent Ising machine*, *Sci. Adv.* **7**, eabh0952 (2021).
 - [31] W. Asavanant, Y. Shiozawa, S. Yokoyama, B. Charoen-sombutamon, H. Emura, R. N. Alexander, S. Takeda, J.-i. Yoshikawa, N. C. Menicucci, H. Yonezawa, *et al.*, *Generation of time-domain-multiplexed two-dimensional cluster state*, *Science* **366**, 373 (2019).
 - [32] M. V. Larsen, X. Guo, C. R. Breum, J. S. Neergaard-Nielsen, and U. L. Andersen, *Deterministic generation of a two-dimensional cluster state*, *Science* **366**, 369 (2019).
 - [33] M. V. Larsen, X. Guo, C. R. Breum, J. S. Neergaard-Nielsen, and U. L. Andersen, *Deterministic multi-mode gates on a scalable photonic quantum computing platform*, *Nat. Phys.* **17**, 1018 (2021).
 - [34] D. Frustaglia, J. P. Baltanás, M. C. Velázquez-Ahumada, A. Fernández-Prieto, A. Lujambio, V. Losada, M. J. Freire, and A. Cabello, *Classical physics and the bounds of quantum correlations*, *Phys. Rev. Lett.* **116**, 250404 (2016).
 - [35] S. Abramsky, R. S. Barbosa, G. Carù, and S. Perdrix, *A complete characterization of all-versus-nothing arguments for stabilizer states*, *Philos. Trans. R. Soc. A* **375**, 20160385 (2017).
 - [36] V. Scarani, A. Acín, E. Schenck, and M. Aspelmeyer, *Nonlocality of cluster states of qubits*, *Phys. Rev. A* **71**, 042325 (2005).
 - [37] W. Tang, S. Yu, and C. Oh, *Greenberger–Horne–Zeilinger paradoxes from qudit graph states*, *Phys. Rev. Lett.* **110**, 100403 (2013).
 - [38] Z.-H. Liu, J. Zhou, H.-X. Meng, M. Yang, Q. Li, Y. Meng, H.-Y. Su, J.-L. Chen, K. Sun, J.-S. Xu, *et al.*, *Experimental test of the Greenberger–Horne–Zeilinger-type paradoxes in and beyond graph states*, *npj Quantum Information* **7**, 66 (2021).
 - [39] L. Lovász, *On the Shannon capacity of a graph*, *IEEE Trans. Inf. Theory* **25**, 1 (1979).
 - [40] A. Cabello, M. Kleinmann, and C. Budroni, *Necessary and sufficient condition for quantum state-independent contextuality*, *Phys. Rev. Lett.* **114**, 250402 (2015).
 - [41] L. Hardy, *Nonlocality for two particles without inequalities for almost all entangled states*, *Phys. Rev. Lett.* **71**, 1665 (1993).
 - [42] N. D. Mermin, *The best version of Bell’s theorem*, *Ann. N. Y. Acad. Sci.* **755**, 616 (1995).
 - [43] E. Amsalem, L. E. Danielsen, A. J. López-Tarrida, J. R. Portillo, M. Bourennane, and A. Cabello, *Experimental fully contextual correlations*, *Phys. Rev. Lett.* **108**, 200405 (2012).
 - [44] A. A. Klyachko, M. A. Can, S. Binicioğlu, and A. S. Shumovsky, *Simple test for hidden variables in spin-1 systems*, *Phys. Rev. Lett.* **101**, 020403 (2008).
 - [45] A. Cabello, P. Badziag, M. T. Cunha, and M. Bourennane, *Simple Hardy-like proof of quantum contextuality*, *Phys. Rev. Lett.* **111**, 180404 (2013).
 - [46] G. Kirchmair, F. Zähringer, R. Gerritsma, M. Kleinmann, O. Gühne, A. Cabello, R. Blatt, and C. F. Roos, *State-independent experimental test of quantum contextuality*, *Nature* **460**, 494 (2009).
 - [47] B. Marques, J. Ahrens, M. Nawareg, A. Cabello, and M. Bourennane, *Experimental observation of Hardy-like quantum contextuality*, *Phys. Rev. Lett.* **113**, 250403 (2014).
 - [48] M. Jerger, Y. Reshitnyk, M. Oppliger, A. Potočnik, M. Mondal, A. Wallraff, K. Goodenough, S. Wehner, K. Juliusson, N. K. Langford, *et al.*, *Contextuality without nonlocality in a superconducting quantum system*, *Nat. Commun.* **7**, 12930 (2016).
 - [49] N. D. Mermin, *Hidden variables and the two theorems of John Bell*, *Rev. Mod. Phys.* **65**, 803 (1993).
 - [50] M. Perkel, *Bounding the valency of polygonal graphs with odd girth*, *Can. J. Math.* **31**, 1307 (1979).
 - [51] L. Lovász, M. Saks, and A. Schrijver, *Orthogonal representations and connectivity of graphs*, *Linear Algebra Its Appl.* **114**, 439 (1989).
 - [52] R. Fickler, R. Lapkiewicz, W. N. Plick, M. Krenn, C. Schaeff, S. Ramelow, and A. Zeilinger, *Quantum entanglement of high angular momenta*, *Science* **338**, 640 (2012).
 - [53] E. A. Aguilar, M. Farkas, D. Martínez, M. Alvarado, J. Cariñe, G. B. Xavier, J. F. Barra, G. Cañas, M. Pawłowski, and G. Lima, *Certifying an irreducible 1024-dimensional photonic state using refined dimension witnesses*, *Phys. Rev. Lett.* **120**, 230503 (2018).
 - [54] M. Yang, Y. Xiao, Y.-W. Liao, Z.-H. Liu, X.-Y. Xu, J.-S. Xu, C.-F. Li, and G.-C. Guo, *Zonal reconstruction of photonic wavefunction via momentum weak measurement*, *Laser & Photonics Reviews* **14**, 1900251 (2020).
 - [55] S. Yokoyama, R. Ukai, S. C. Armstrong, C. Sornphiphat-phong, T. Kaji, S. Suzuki, J.-i. Yoshikawa, H. Yonezawa, N. C. Menicucci, and A. Furusawa, *Ultra-large-scale continuous-variable cluster states multiplexed in the time domain*, *Nat. Photon.* **7**, 982 (2013).
 - [56] S. Bartolucci, P. Birchall, H. Bombin, H. Cable, C. Dawson, M. Gimeno-Segovia, E. Johnston, K. Kieling, N. Nickerson, M. Pant, *et al.*, *Fusion-based quantum computation* (2021), [arXiv:2101.09310](https://arxiv.org/abs/2101.09310).
 - [57] A. M. Gleason, *Measures on the closed subspaces of a Hilbert space*, *J. Math. Mech.* **6**, 885 (1957).
 - [58] R. P. Feynman, *Simulating physics with computers*, *Int.*

- J. Theor. Phys. **21**, 467 (1982).
- [59] A. Cabello, M. Gu, O. Gühne, and Z.-P. Xu, *Optimal classical simulation of state-independent quantum contextuality*, *Phys. Rev. Lett.* **120**, 130401 (2018).
 - [60] L. S. Madsen, F. Laudenbach, M. F. Askarani, F. Rortais, T. Vincent, J. F. Bulmer, F. M. Miatto, L. Neuhaus, L. G. Helt, M. J. Collins, *et al.*, *Quantum computational advantage with a programmable photonic processor*, *Nature* **606**, 75 (2022).
 - [61] A. Cabello, *Converting contextuality into nonlocality*, *Phys. Rev. Lett.* **127**, 070401 (2021).
 - [62] S. Weidemann, M. Kremer, T. Helbig, T. Hofmann, A. Stegmaier, M. Greiter, R. Thomale, and A. Szameit, *Topological funneling of light*, *Science* **368**, 311 (2020).
 - [63] C. Leefmans, A. Dutt, J. Williams, L. Yuan, M. Parto, F. Nori, S. Fan, and A. Marandi, *Topological dissipation in a time-multiplexed photonic resonator network*, *Nat. Phys.* **18**, 442 (2022).
 - [64] M. Grötschel, L. Lovász, and A. Schrijver, *The ellipsoid method and its consequences in combinatorial optimization*, *Combinatorica* **1**, 169 (1981).
 - [65] R. C. Bose, *Strongly regular graphs, partial geometries and partially balanced designs.*, *Pac. J. Math.* **13**, 389 (1963).
 - [66] D. G. Higman, *Finite permutation groups of rank 3*, *Math. Z.* **86**, 145 (1964).
 - [67] P. Delsarte, *Weights of linear codes and strongly regular normed spaces*, *Discrete Math.* **3**, 47 (1972).
 - [68] D. M. Cvetković, M. Doob, and H. Sachs, *Spectra of graphs* (Academic Press Inc. [Harcourt Brace Jovanovich Publishers], New York, 1980) p. 115.
 - [69] P. Delsarte, *An algebraic approach to the association schemes of coding theory*, *Philips Res. Rep. Suppl.* **10**, vi+ (1973).
 - [70] P. Delsarte, *Sur le théorème de tait*, *L'Intermédiaire des Mathématiciens* **5**, 225 (1898).
 - [71] A. Clebsch, *Ueber die flächen vierter ordnung, welche eine doppelcurve zweiten grades besitzen.*, *Journal für die reine und angewandte Mathematik* **69**, 142 (1868).
- Acknowledgements.**—We thank Adán Cabello for inspiring discussion. This work was supported by the Innovation Program for Quantum Science and Technology (Grant No.2021ZD0301400), the National Natural Science Foundation of China (Grants Nos.61725504, 11774335, 11821404, and U19A2075), the Fundamental Research Funds for the Central Universities (Grant Nos.WK2030380017 and WK2030000056), and the Anhui Initiative in Quantum Information Technologies (Grant Nos.AHY020100, and No.AHY060300). J.M. was supported in part by the National Key R and D Program of China (Grant No.2020YFA0713100), National Natural Science Foundation of China (Grant No.12125106), Innovation Program for Quantum Science and Technology (Grant No.2021ZD0302904), and Anhui Initiative in Quantum Information Technologies (Grant No.AHY150200). J.L.C. was supported by the National Natural Science Foundations of China (Grant Nos.11875167 and 12075001). Z.-P. X. was supported by the Alexander Humboldt foundation.
- Author contributions.** Z.-H.L., Y.M., and Y.-Z.W. contributed equally to this work.

Extended Data Figure 2. **Detailed experimental setup.** The blue lines denote optical fibres, and the red strokes indicate light propagating in free-space sessions. Electronic connections are denoted by grey lines. The beam-splitter ports marked with the same colour have higher transmissivity. Acronyms: AFG arbitrary function generator, IM intensity modulator, Osc. oscilloscope, PM phase modulator, PZT piezoelectric fibre stretcher.



Extended Data Figure 3. **Detector response curve.** The data points denote the balanced homodyne detector's voltage response to the power difference between two input ports. The curve is a linear fit of the data points which have power differences below 5 μW . The histogram shows the distribution of the power differences of the data points registered during the experiment; the maximal power difference was 3.05 μW and all data points fell in the linear response range.